This is an open access article published under an ACS AuthorChoice License, which permits copying and redistribution of the article or any adaptations for non-commercial purposes.

ACS OMEGA

Article

Cite This: ACS Omega 2018, 3, 2130−2140

Reassessment of the Four-Point Approach to the Electron-Transfer Marcus−Hush Theory

Omar López-Estrada,* Humberto G. Laguna, Cihuapilli Barrueta-Flores, and Carlos Amador-Bedolla*

Departamento de Física y Química Teórica, Facultad de Química, Universidad Nacional Autónoma de México, Av. Universidad 3000, Ciudad Universitaria, CP 04510 Ciudad de México, Mexico

Supporting Information

ABSTRACT: The Marcus−Hush theory has been successfully applied to describe and predict the activation barriers and hence the electron-transfer (ET) rates in several physicochemical and biological systems. This theory assumes that in the ET reaction, the geometry of the free Gibbs energy landscape is parabolic, with equal curvature near the local minimum for both reactants and products. In spite of its achievements, more realistic models have included the assumption of the two parabolas having not the same curvature. This situation is analyzed by the Nelsen's four-point method. As a benchmark to compare the Marcus−Hush approximation to a precise calculation of the excitation energy, we studied the non-ET process of the electronic excitation of the aluminum dimer that has two local minima ($^3\sum_g^-$ and $^3\prod_u$ electronic states) and allows to obtain analytically the Marcus−Hush nonsymmetric parameters. We appraise the ability of the Marcus−Hush formula to approximate the analytical results by using several averages of the two reorganization energies associated with the forward and backward transitions and analyze the error. It is observed that the geometric average minimizes the relative error and that the analytical case is recovered. The main results of this paper are obtained by the application of the Nelsen's four-point method to compute the reorganization energies of a large set of potential π-conjugated molecules proposed for organic photovoltaic devices using the above-mentioned averages for the Marcus−Hush formula. The activation energies obtained with the geometric average are significantly larger for some donor−acceptor pairs in comparison with the previously employed arithmetic average, their differences being suitable for experimental testing.

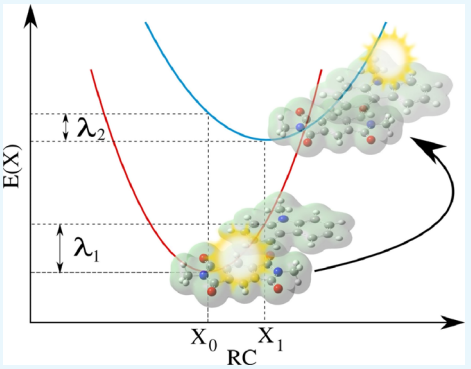

INTRODUCTION

The longstanding interest on the electron-transfer (ET) process[1−4] relies on its influence within a plethora of physicochemical and biological phenomena, such as electrochemical reactions,[5−12] DNA damage and repair,[13−16] interactions between peptides and other macromolecules,[17−20] photosynthesis,[21] biochemical processes,[22−24] model systems,[25,26] and the technological interest on the exciton transfer in organic photovoltaics.[27−55]

Historically, the theoretical models to understand ET can be traced back to the pioneer work of Marcus[5−8,56,57] and Hush.[58,59] The Marcus−Hush theory exhibits a mutual dependence of the ET rate (k_{ET}) and the reaction free energy (ΔG^0).[60] As a consequence, the theory exhibits a maximum of the reaction rate when $-\Delta G^0$ is equal to the reorganization energy λ. Thus, there exists a region where the increase of the reaction driving force ΔG^0 (reactants → products) leads to an increase in k_{ET}, which is known as the Marcus normal region. Additionally, the theory exhibits a region where the increase of the driving force results in a decrease in the reaction rate, that is, when $-\Delta G^0 > \lambda$, which is known as the Marcus inverted region.[60−62] Remarkably, the activation free energy $\Delta G^\dagger$ can be calculated from the reorganization energy λ and the driving force ΔG^0.

A first assumption of the Marcus−Hush theory is to consider that the electron is transferred only when the reactant and product states have the same energy, as required by the Franck−Condon approximation and the energy conservation principle in the absence of interaction with external energy sources (such as photons). This equi-energetic situation (stabilization of products or destabilization of reactants) required by the Marcus−Hush model is due to environment fluctuations.[63] The second assumption is that the solvent response to variations in molecular densities is linear around the relaxed state; hence, the free energy is quadratic. This has two consequences. On the one hand, the free energies can be modeled by two parabolas centered at the stable states of reactants and products. On the other hand, these two parabolas have the same curvature,[64] indicating that the two reorganization energies (products → reactants and reactants → products) are the same.

Despite the hard assumption that both parabolas have the same curvature, the Marcus−Hush theory is both qualitatively and quantitatively accurate for most systems. However, in

Received: September 25, 2017
Accepted: February 8, 2018
Published: February 21, 2018

© 2018 American Chemical Society

DOI: 10.1021/acsomega.7b01425
ACS Omega 2018, 3, 2130−2140

general, it is known that the solvent response is nonlinear and that it manifests through differences between the curvatures of the parabolas.[63] Even in such a situation, the Marcus−Hush theory fits as a first approximation that can give consistent predictions.[63,65,66] In spite of the previous mentioned achievements, many important cases are known where the equal curvature assumption fails and several attempts to generalize the Marcus−Hush theory have been reported.[8−12,63,65−69] The inclusion of different curvatures to account for nonlinear solvent responses as well as other internal molecular features has been previously discussed[8−12,63,65−69] but is still an open problem.

The reorganization energy λ is normally split into internal (λ_i) and external or "outer" (λ_o) contributions. The internal reorganization energy λ_i accounts for changes in bond lengths and other structural parameters of the molecules. In gas-phase reactions, it is the only contribution to the system reorganization energy. In this sense, λ_i can be achieved by quantum mechanical calculations.[31,70−76] The external term, λ_o, comes from the contributions of the solvent molecules to the reorganization energy, and in condensed phase reactions (liquids or solids), this term becomes dominant. Explicit consideration of solvent−molecule interactions makes the system quantum mechanically intractable, hence λ_o is often calculated by means of classical dynamics methodologies or by employing implicit solvent quantum mechanical models.

Regardless of this complication in computing λ_o, an exceptional effort has been done to calculate λ_i, and many quantum mechanical schemes have been introduced.[31,70−77] One of the methods most often employed is the four-point scheme proposed by Nelsen,[77] which has been extensively applied because of its simplicity and it has been successfully proven for many systems.[72,73,78−90] Particularly, it has been used in the computation of electron self-exchange reactions.[83,85,90] In such a scheme, the Marcus−Hush theory provides a method to find the intersection between the two parabolas by means of the knowledge of just four points in the free energy surface. Two points are the free energy of reactants and products in their respective local minima geometry, and the other two points are obtained by computing the free energy at the reactants' geometry in the potential energy surface (PES) of the products and vice versa. In this scheme, the energetic differences between the molecules in their stable and nonstable states are related with two reorganization energies (λ_1 and λ_2).

In this work, we analyze several averages of these two reorganization energies as a method to generalize the Marcus−Hush theory to include parabolas with different curvatures, as has been tried in previous reports.[85,90] In such an attempt, we discuss the error of employing the distinct averages in a model system of an aluminum dimer, which has been extensively investigated both experimentally[91] and theoretically.[92] This simple model, while not an ET system, allows us to explore analytically the reorganization energies as well as the driving force by noting that the Marcus−Hush theory can be seen as a method to find the intersection between the parabolas along the reaction coordinate. The analysis of the relative error allows us to explore novel donor and acceptor molecules used in organic photovoltaics by means of the averaged reorganization energy.

The rest of the paper is organized as follows. In section II, we outline the Marcus−Hush theory. In section III, Results and Discussion, a simple diatomic model is analytically solved and the ability of the Marcus−Hush theory to recover the analytic solution is appraised, also we analyze the ability of four different averages of the parabolic curvatures to capture the analytic solution obtained for the aluminum benchmark system. Next, we apply our findings to analyze the activation energy prediction for photovoltaic donor−acceptor (D−A) pairs and report results that can be relevant in applications. Finally, in section IV, conclusions are presented.

OUTLINE OF THE MARCUS−HUSH THEORY

The Marcus−Hush theory schematic view of the system is shown in Figure 1. The PES geometry near the local minimum,

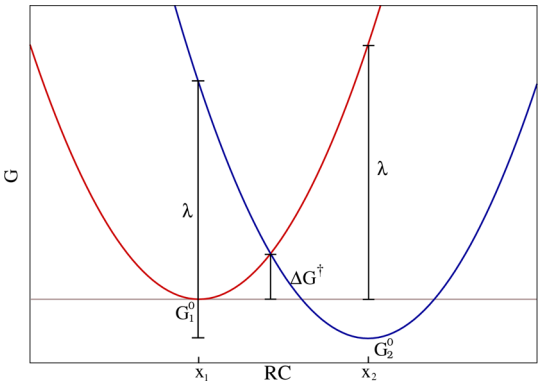

Figure 1. Idealized parabolic PESs for reactants ($G_1(x)$, red) and products ($G_2(x)$, blue) in the electron self-exchange process, $M^- \leftrightarrow M$, as functions of the reaction coordinate. The two parabolas have the same curvature near the respective local minimum (x_1 and x_2). The activation energy $\Delta G^\dagger$ is given by the reorganization energy λ and the driving force $\Delta G^0 = G_2^0 - G_1^0$.

for either reactants (red) or products (blue), is approximated by a parabola with a defined curvature k. It is assumed that the species involved in the reaction are structurally relaxed in their respective initial (x_1) and final (x_2) reaction coordinate values. Moreover, the physical situation is the guess that both local minima of reactants and products are connected along an assumed reaction pathway, described by a complex N-dimensional specific reaction coordinate direction on the PES.

In accordance with Figure 1, the corresponding parabolic equations are

$$G_1(x) = G_1^0 + k(x - x_1)^2,$$
$$G_2(x) = G_2^0 + k(x - x_2)^2 \quad (1)$$

and their intersection at $x^\dagger$ defines the potential energy barrier as

$$\Delta G^\dagger = G_1(x^\dagger) - G_1^0 = \frac{(\Delta G^0 + \lambda)^2}{4\lambda} \quad (2)$$

with the definitions $\Delta G^0 = G_2^0 - G_1^0$ and $\lambda = k(x_2 - x_1)^2$, where λ stands for the reorganization energy. Application of the Marcus−Hush theory implies the knowledge of merely $k(x_1 - x_2)$ and remarkably not of the individual reaction coordinates. The reorganization energy can be evaluated by

$$G_2(x_1) - G_1(x_1) = \lambda + \Delta G^0 \text{ or}$$
$$G_1(x_2) - G_2(x_2) = \lambda - \Delta G^0 \quad (3)$$

DOI: 10.1021/acsomega.7b01425
ACS Omega 2018, 3, 2130−2140

Also, in the case of two parabolas not having the same curvature ($k_1 \neq k_2$), the intersection between the curves can be analytically found. In this case, the activation energy is strongly related both to the reorganization energy previously mentioned λ_1 (reactants → products) and to a new defined reorganization energy λ_2 obtained in the reverse direction (products → reactants).

However, the analytical solution cannot be written in terms of neither λ_1 nor λ_2. Rather the intersection is related to the free activation energy $\Delta G^{\dagger}$, so an approximate solution for $k_1 \approx k_2$ can be achieved by means of a Taylor expansion, giving the corresponding transition state energy

$$\Delta G_{+}^{\dagger} = k_1 \frac{(\Delta G^0 + k_1 x_1^{\,2} + k_2 x_2^{\,2} - 2k_2 x_1 x_2)^2}{4(k_2 x_2 - k_1 x_1)^2} \tag{4}$$

One can easily notice that eq 4 leads to the Marcus–Hush formula (eq 2) when $k_1 = k_2 = k_3$. Hence, the Marcus–Hush formula can be seen as an approximation to the analytical solution for small differences between λ_1 and λ_2. A detailed discussion on the analytical and approximate solutions can be found in the Supporting Information.

To apply the above scheme to an ET process, we first consider an electron self-exchange reaction

$$M^- \leftrightarrow M \tag{5}$$

and denote by $\lambda_I(M)$ and $\lambda_{II}(M)$ the reorganization energies of the forward and backward reactions, respectively, and the reaction driving force is $\Delta G \neq 0$, as depicted in Figure 2. The reorganization energy $\lambda_I(M)$ is the required energy to reach the geometry of the products from the geometry of the reactants without transferring the electron, whereas $\lambda_{II}(M)$ is the energy required to achieve the positions of the atoms in the reactant complexes from the product geometry without ET. Such reorganization energies are typically different, as schematized in Figure 2. Those cases with very dissimilar λ_I and λ_{II} are examples where one ET deeply influences the relaxed geometry of the isolated donor or acceptor molecules.

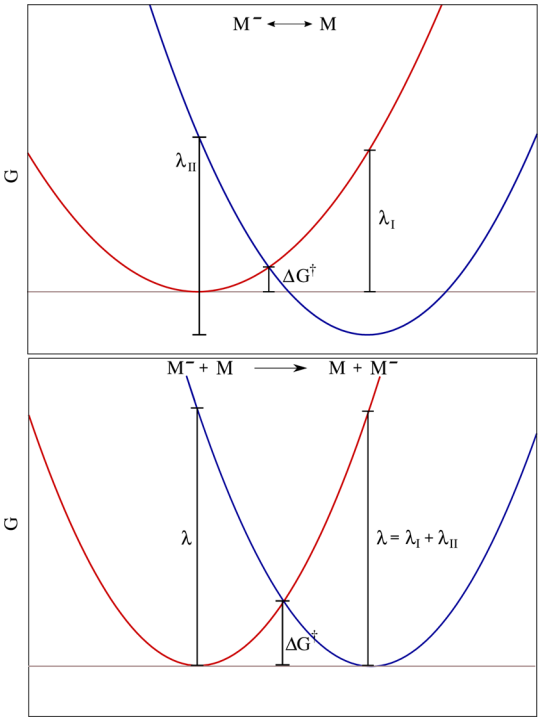

Figure 2. Parabolic PESs for reactants (red) and products (blue) in an electron self-exchange process as a function of the reaction coordinate. Top: $M^- \leftrightarrow M$. Bottom: $M^- + M \rightarrow M + M^-$. $\Delta G^{\dagger}$ is not obtained by only the value of λ_I, but a new reorganization energy λ_{II} must be considered.

Computation of the activation energy of reaction in eq 5 faces the disadvantage that the curvature of the two parabolas could be different and that the application of the Marcus–Hush formula is dubious; notwithstanding, we could try to estimate the activation energy by the substitution of either λ_I or λ_{II} in eq 2. However, a better approach is to construct two parabolas of equal curvature to guarantee the validity of eq 2. As can also be seen in Figure 2, in this case, the equal curvature condition of the Marcus–Hush theory is fulfilled by considering the electron self-exchange process

$$M^- + M \rightarrow M + M^- \tag{6}$$

whose total reorganization energy is the same for the forward and backward directions and can be calculated considering the adduct of the two molecules or by considering them as noninteracting species. We adopt the second approach and compute an approximation to this reorganization energy as the sum of their respective $\lambda_I(M)$ and $\lambda_{II}(M)$[85,90]

$$\lambda(M) = \lambda_I(M) + \lambda_{II}(M)$$

while the driving force is $\Delta G^0 = 0$, thus substitution of $\lambda(M)$ in eq 2 leads to $\Delta G^{\dagger} = \lambda(M)/4$. Hence, a reliable option to estimate the reorganization energy of the reaction in eq 5 is by means of different averages of $\lambda_I(M)$ and $\lambda_{II}(M)$ (arithmetic,[85] harmonic, or geometric) to use eq 2.

Let us now consider a general ET reaction

$$D^- + A \rightarrow D + A^- \tag{7}$$

with D and A denoting donor and acceptor species, respectively, and D^- and A^- their ionized counterparts. This reaction can be split into two electron self–exchange processes, and then the total free energy for their respective local minima G_1^0 and G_2^0 is obtained as the sum of both systems (donor plus acceptor).

$$\lambda_1 = \lambda_1(D, A) = \lambda_I(D) + \lambda_I(A)$$

and

$$\lambda_2 = \lambda_2(D, A) = \lambda_{II}(D) + \lambda_{II}(A)$$

where λ_1 and λ_2 denote the reorganization energies of the forward and backward reactions, respectively, and the reaction driving force, $\Delta G^0 \neq 0$.

The total reorganization energy of this bimolecular system can also be obtained as the different averages of λ_1 and λ_2, similar to the electron self-exchange process.

Before we consider D–A systems, in the next section, we focus on a system that can be solved analytically, followed by Marcus–Hush parameters, and then we test the averages by computing the error with respect to the exact result.

RESULTS AND DISCUSSION

Analytic Marcus–Hush Parameters for Al_2. To study the relevant aspects of the Marcus–Hush theory, a simple diatomic aluminum system has been employed. This example does not correspond to an ET reaction, but it helps to analyze the case of two parabolas with different curvatures. It is worth to mention that while the Marcus transition state theory is most

DOI: 10.1021/acsomega.7b01425
ACS Omega 2018, 3, 2130–2140

broadly used for ET, it is not limited to ET systems and is applicable to almost any nonadiabatic process. Al_2 has been observed to have two local minima both experimentally[91] and theoretically.[92] The spectroscopy experiment reports a $^3\prod_u$ electronic ground state with a bond length of 2.7011 ± 0.0015 Å and a vibrational frequency of 285.80 cm^{-1}. Similarly, a $^3\sum_g^-$ electronic state with a bond length of 2.4665 ± 0.0024 Å and a vibrational frequency of 350.01 cm^{-1} has been reported. Figure 3 shows an energy scan at the Perdew, Burke, and Ernzerhof[93]/

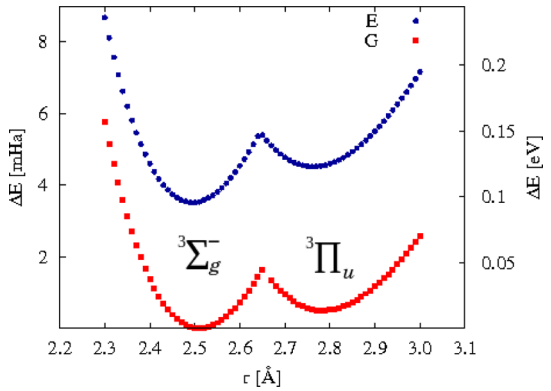

Figure 3. PESs employing the total energy (E, in mHa) and the free Gibbs energy (G, in mHa) for Al_2 as a function of the interatomic distance (r in Å). For an easy visualization, an energy shift has been introduced in the total energy (adding −18.5 mHa). Energy is referred to the ground state.

triplet zeta basis set[94] theory level as previously reported[92] for the triplet PES employing the Gaussian 09 suite,[95] with two well-defined parabolas near each local minima. Despite knowing that the energy order of the local minima for both electronic states is wrongly predicted by density functional theory (DFT) methods, we can analyze the local geometry as the normal modes are real[91,92] after vibrational analysis. Both parabolic equations $y = ax^2 + bx + c$ can be easily obtained for their respective local minima. The coefficients are summarized in Table 1, and the plots employing the coefficients are shown in Figure 3 for both electronic states. The relevant Marcus–Hush parameters were analytically obtained and presented in Table 2.

Table 1. Coefficients of the $y = ax^2 + bx + c$ Equations for the $^3\sum_g^-$ and $^3\prod_u$ Electronic State System Employing the Total Energy, E (in Ha), and the Free Gibbs Energy, G (in Ha)

	E		G	
	$^3\sum_g^-$	$^3\prod_u$	$^3\sum_g^-$	$^3\prod_u$
A	0.11853	0.07440	0.11557	0.05711
b	−0.59468	−0.41265	−0.58337	−0.32101
c	−483.876	−484.049	−483.795	−484.079

Starting from the $^3\sum_g^-$ electronic state, the bonding distance can be increased to reach the intersection point. The energy barrier is determined by the intersection point coordinates ($x^\dagger$, $G(x^\dagger)$). In this particular example, we need to know only the dimer bond distance as the reaction coordinate results from the knowledge of both analytical functions, and therefore, the reorganization energy λ is not necessary to be applied in the Marcus–Hush model.

Table 2. Coordinates of the Minimum for the $^3\sum_g^-$ and $^3\prod_u$ Electronic States of the Al_2 System, x_i (in Å) and G_i^0 (in Ha) in Each Parabola[a]

i	x_i	G_i^0	k_i	λ_i
$^3\sum_g^-$	2.524	−484.5311	0.1186	9.51 (10^{-3})
$^3\prod_u$	2.811	−484.5304	0.0571	4.70 (10^{-3})

[a]The curvature k_i and the reorganization energy λ_i (in Ha) are analytically obtained.

The activation energy from the Marcus–Hush formula can be evaluated with different averages of the reorganization energies. λ_1 is used to estimate $\Delta G^\dagger$ when the system is going from reactants to products, and λ_2 appears when the system reaches the minimum of the reactants starting from the PES of the products. We will consider the arithmetic ($\bar{\lambda}_1$), harmonic ($\bar{\lambda}_2$), and geometric ($\bar{\lambda}_3$) averages, and the arithmetic average of the first two ($\bar{\lambda}_4$)

$$\bar{\lambda}_1 = \frac{(\lambda_1 + \lambda_2)}{2} \tag{8}$$

$$\bar{\lambda}_2 = \frac{(2\lambda_1\lambda_2)}{(\lambda_1 + \lambda_2)} \tag{9}$$

$$\bar{\lambda}_3 = \sqrt{\lambda_1\lambda_2} \tag{10}$$

$$\bar{\lambda}_4 = \frac{(\bar{\lambda}_1 + \bar{\lambda}_2)}{2} \tag{11}$$

Because the reaction coordinates in the $\lambda = k(x_2 - x_1)^2$ equation are known for the Al_2 system, for the purpose of explaining the error of the different averages, we will consider the curvature k and not the reorganization energy λ as follows.

To delve into the general behavior for arbitrary variations of the ratio k_1/k_2 between parabolas and to analyze the error in such hypothetical cases, defined as

$$\text{error} = \frac{\Delta G^\dagger_{\text{analytical}} - \Delta G^\dagger(\lambda_i)_{\text{calc}}}{\Delta G^\dagger_{\text{analytical}}} \tag{12}$$

we plot the relative error (Figure 4) employing the Marcus–Hush formula for the different k's as a function of the curvature ratio of both parabolas ($k_2 = 0.057411$ is fixed and k_1 is varied). For the Al_2 system, the ratio $k_1/k_2 \approx 2.02$. The error percentage is obtained by multiplying the relative error by 100 and taking the absolute value.

It is observed that employing an average of the curvature k, the error is decreased in comparison with using either k_1 or k_2 (Figure 4), for $k_1/k_2 \leq 2$, all the averages give errors of less than 5%, whereas k_1 and k_2 separate immediately one from the other. Besides, in spite of the fact that the relative error is nonzero for all the curvatures explored, there are few regions where the error decreases as seen in the bottom plot, where data with error less than 5% and up to the ratio $k_1/k_2 = 3$ are displayed. It is also observed that the geometrical average $\bar{k}_3$ and the average of average $\bar{k}_4$ depart slowly from zero error, specially they seem to be the best choices for larger values of the ratio k_1/k_2. It is worth to mention that $\bar{k}_4$ is obtained from two averages. For a better understanding of the error percentage, the activation energies $\Delta G^\dagger$ are computed (Table 3) for their respective reorganization energy and compared with the analytical value obtained. It exhibits the good agreement of the error obtained with $\bar{k}_3$ and $\bar{k}_4$ averages in comparison to the previous error

DOI: 10.1021/acsomega.7b01425
ACS Omega 2018, 3, 2130–2140

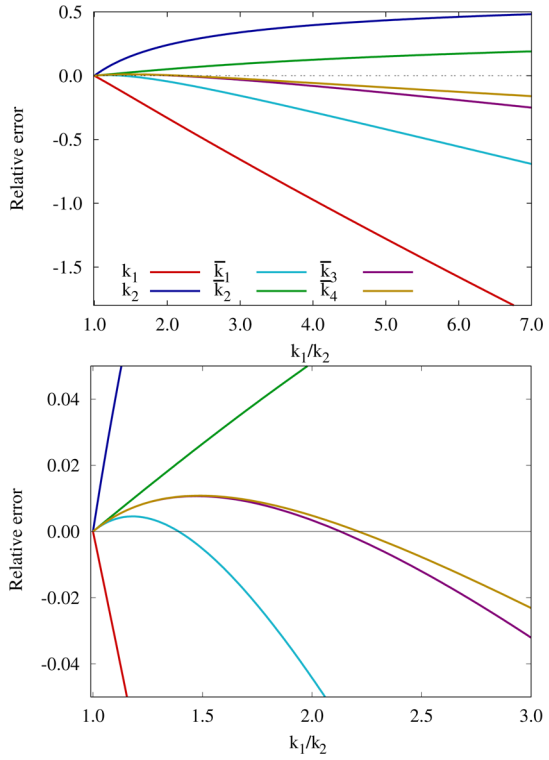

Figure 4. Top: Variation of the relative error in the calculation of the transition state energy ($\Delta G^{\dagger}$) from the Marcus–Hush formula with different curvatures: k_1, k_2, $\overline{k}_1$, $\overline{k}_2$, $\overline{k}_3$, $\overline{k}_4$ as a function of the curvature ratio, k_1/k_2, for fixed k_2 = 0.05711. Bottom: Detail of the previous plot. Percentage can be obtained from the plots (see text).

Table 3. Activation Energy (in mHa) and Percentage Error in the Marcus–Hush Formula Using Eq 2 with Different λ's[a]

	$\Delta G^{\dagger}$	% err
	2.044	
λ_1	2.736	33.87
λ_2	1.546	24.36
$\overline{\lambda}_1$	2.139	4.65
$\overline{\lambda}_2$	1.937	5.21
$\overline{\lambda}_3$	2.038	0.28
$\overline{\lambda}_4$	2.035	0.43

[a]The first row corresponds to the analytical value.

discussed. Employing either $\overline{k}_3$ or $\overline{k}_4$ averages, the relative error is minimized and the closest value to the analytical activation energy $\Delta G^{\dagger}$ is obtained.

Organic Photovoltaic Systems. One of the branches with greater relevance to apply the ET Marcus–Hush theory is the process between a donor and an acceptor molecule in an organic photovoltaic (OPV) cell.[31,75,76] In this work, a set of potential molecules (Figure 5) for OPV devices are employed to assess the Nelsen's four-point method and verify the best choice of the reorganization energy in accordance with the Al_2 dimer discussion.

With this purpose, we use the list of molecules compiled by Das and Ghosh[96] functionalized in all their R-positions with methyls, and we did not consider another substituent. Also, while it is known that only few of the possible pairs are suitable D–A systems in the experiment,[96] for the sake of completeness of our analysis, we considered all possible combinations (120 D–A pairs). At the end of the section, we present D–A pairs that have energy barriers potentially attainable for practical applications; nevertheless, in the following discussion, we do not restrict ourselves to these pairs.

The total reorganization energies of the D–A system are treated as two contributions separately.[77] Each molecule is individually geometry-relaxed without considering solvent interactions. Details of the computations are given in the Methods section at the end of this text. A summary of the total energy and free Gibbs energy is reported in the Supporting Information, Tables S2 and S3.

The activation energy $\Delta G^{\dagger}$ is computed for each D–A system employing either λ_1, λ_2, or the arithmetic and geometric averages $\overline{\lambda}_1$ and $\overline{\lambda}_3$, respectively (the $\overline{\lambda}_2$ and $\overline{\lambda}_4$ averages considered are reported in the Supporting Information). In Figure 6, it can be observed that employing $\Delta G^{\dagger}(\overline{\lambda}_3)$ as our y-axis reference, dispersion between $\Delta G^{\dagger}(\overline{\lambda}_1)$ and $\Delta G^{\dagger}(\overline{\lambda}_2)$ occurs for values higher than 2.0 eV. The activation energy obtained by means of λ_1 is in most cases lower than employing λ_2. Actually, there are several systems where the $\Delta G^{\dagger}(\lambda_2)$ is higher than all the other barriers obtained. Remarkably, the $\Delta G^{\dagger}(\overline{\lambda}_3)$ shows an exceptional correlation for the 120 D–A pairs with respect to $\Delta G^{\dagger}(\overline{\lambda}_1)$.

It is useful to mention that the arithmetic average $\overline{\lambda}_1$ has been previously employed in the computational model of ET in a homogeneous oxidation of aqueous transition-metal ions by dissolved molecular oxygen.[85] In our analysis, the arbitrary choice of either $\overline{\lambda}_1$ or $\overline{\lambda}_3$ seems not to represent a relevant difference and could be indistinctly adopted to calculate the activation energy.

It is instructive to analyze the components of $\Delta G^{\dagger}$ to explain the behavior displayed in Figure 6. The leading term is proportional to the ratio between the squared free energy difference and the reorganization energy, as is shown in Figure S2 of the Supporting Information. In Figure S3, the term proportional to the reorganization energy is shown. The influence of the chosen λ in the computations is apparent through both figures, and their dispersions are consistent with results presented in Figure 6, particularly that of the leading term.

On the other hand, Figure S4 in the Supporting Information displays the poor correlation between $\Delta G^{\dagger}$ data computed with λ_1 or alternatively with λ_2, while Figure S5 shows the almost perfect linear fit among the data computed with $\overline{\lambda}_3$ and with $\overline{\lambda}_4$. Such a linear correlation remarks the arbitrary choice between $\overline{\lambda}_3$ and $\overline{\lambda}_4$.

At this point, we discuss the predicted energetic barrier differences when $\overline{\lambda}_1$ is replaced by $\overline{\lambda}_3$ in the four-point calculation scheme, as shown in Figure 7. Values calculated with $\overline{\lambda}_3$ are larger than those using $\overline{\lambda}_1$, leading to a decrease in the predicted reaction rate. Such energetic differences are suitable to be detected by experiments, as in most cases, that is, in 64 pairs, energetic barrier differences are observed to be larger than 10 meV, whereas in 54 pairs, differences are observed to be larger than 20 meV. In D–A pairs (D2, D4, D5, D6, D7, D8, D9)–A2, (D2, D4, D9)–A3, (D9, D10)–A5, and (D2, D4, D9)–A11, we found differences larger than 100 meV. To facilitate interpretation of the data, the numerical values plotted in Figure 7 are presented in Table S4 of the Supporting Information.

Now, we analyze the qualitative behavior of our results as a function of the ratio λ_1/λ_2. With this aim, we construct relative error plots using various references (assumed true values). In these cases, we can neither calculate the error nor make a

DOI: 10.1021/acsomega.7b01425
ACS Omega 2018, 3, 2130–2140

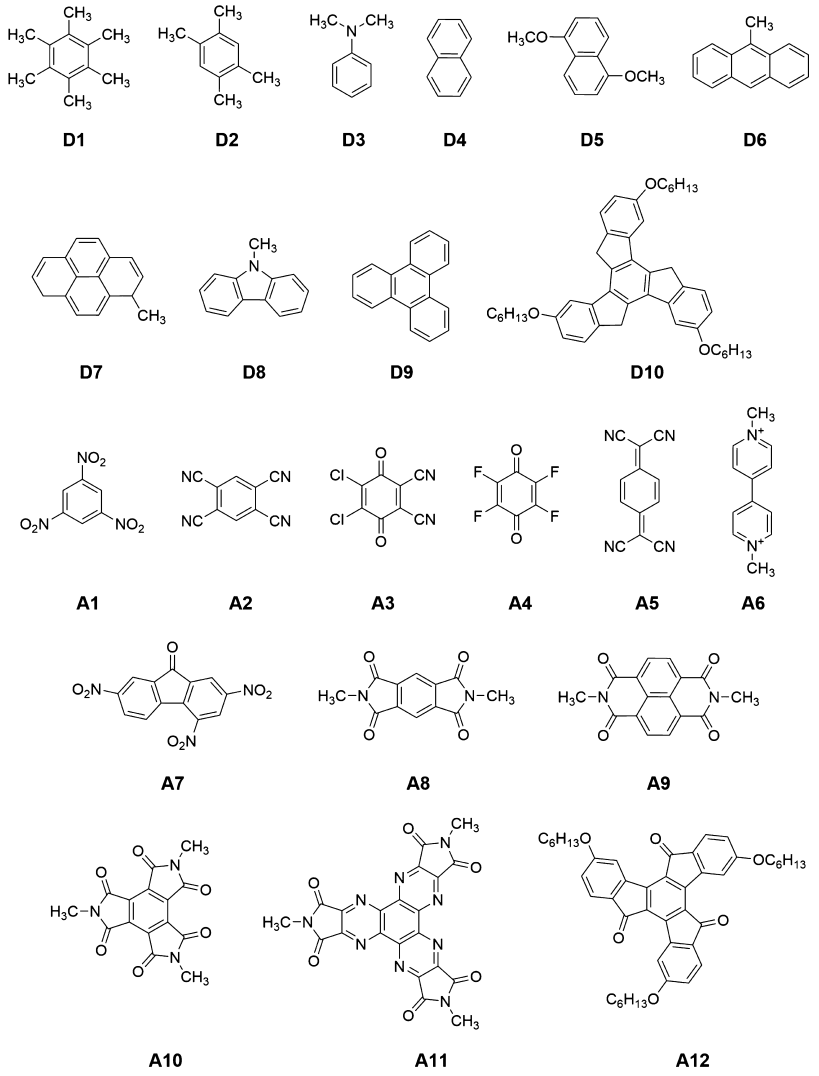

Figure 5. Structures in the set of representative π-donors and acceptors used in this paper.

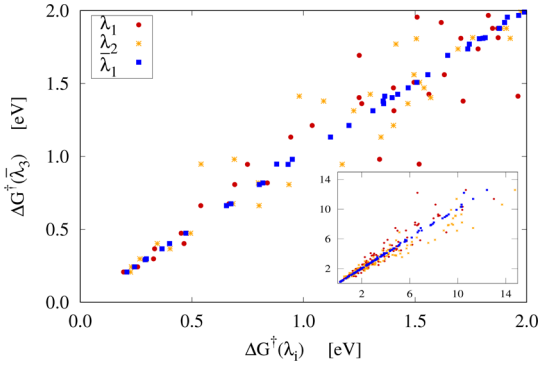

Figure 6. Comparison of $\Delta G^{\dagger}$ calculated with $\bar{\lambda}_1$, λ_1, or λ_2 and those calculated with $\bar{\lambda}_3$. Linear fit equations are as follows: $f(x) = 1.023x - 0.028$, with $R^2 = 0.997$ (blue); $f(x) = 1.049x + 0.097$, with $R^2 = 0.909$ (red); and $f(x) = 0.769x + 0.582$, with $R^2 = 0.914$ (orange). Main plot: Results for 37 pairs with $\Delta G^{\dagger}$ below 2.0 eV. Inset: results for all the 120 pairs including unrealistic $\Delta G^{\dagger}$ up to 14 eV.

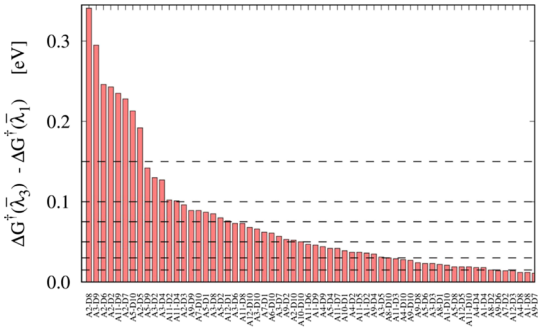

Figure 7. Energy differences $\Delta G^{\dagger}(\bar{\lambda}_3) - \Delta G^{\dagger}(\bar{\lambda}_1)$ of the D−A pairs. Differences larger than 10 meV are shown. The differences for the pair A2−D9 (1.676 eV) and for the pair A2−D4 (0.542 eV) are not shown. Horizontal lines are displayed at 0.015, 0.03, 0.05, 0.075, 0.1, and 0.15, to facilitate interpretation.

variation of the reorganization energies, instead in Figure 8, we plot the error (eq 12) with respect to $\bar{\lambda}_3$. This plot is constructed under the assumption that the only significant feature of the D−A pairs is the ratio of the internal reorganization energies; this hard assumption dismisses all other geometrical parameters that can influence reorganization, such as the number of atoms.

In Figure 8, we split the plot in two regions according to the relative value of λ_1 with respect to λ_2 ($\lambda_1 < \lambda_2$ and $\lambda_1 > \lambda_2$), showing that such an inequality does not influence the

DOI: 10.1021/acsomega.7b01425
ACS Omega 2018, 3, 2130−2140

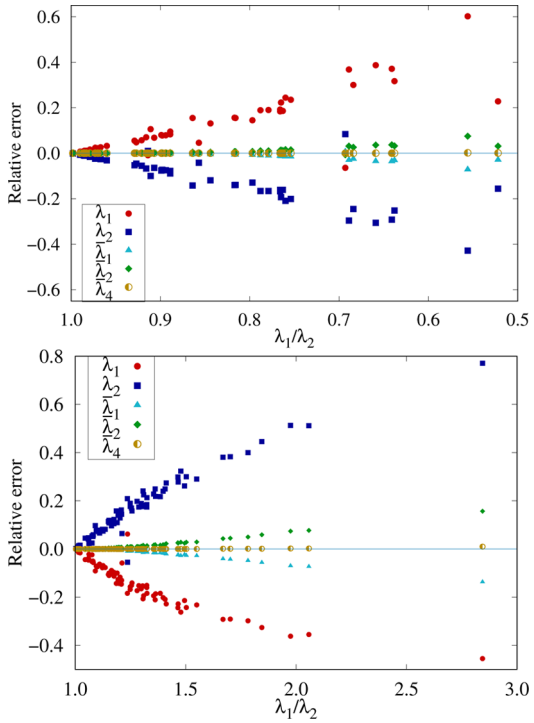

Figure 8. Variation of the relative error in the calculation of the activation energy ($\Delta G^{\dagger}$) from the Marcus–Hush formula with λ_1, λ_2, $\bar{\lambda}_1$, $\bar{\lambda}_2$, and $\bar{\lambda}_4$ with respect to the reference $\bar{\lambda}_3$, as a function of the reorganization energy ratio, λ_1/λ_2. Values for all the 120 D–A pairs are shown. Top: $\lambda_1 < \lambda_2$ case. Bottom: $\lambda_1 > \lambda_2$ case.

qualitative behavior of the plots: both regions display very similar trends. We observe that $\bar{\lambda}_4$ values are the closest to zero error because of their almost perfect linear fit (see Figure S5 in the Supporting Information), which is also consistent with the Al_2 dimer. Using the other averages $\bar{\lambda}_1$ or $\bar{\lambda}_2$, we get smaller errors than using the internal reorganization energies λ_1 or λ_2, also in accordance with the benchmark.

As discussed above, the activation energy computed with λ_1 is lower than that with $\bar{\lambda}_3$ for the case $\lambda_1 > \lambda_2$ (negative relative error, bottom plot in Figure 8), whereas it is larger for the case $\lambda_1 < \lambda_2$ (positive relative error, top plot). Few exceptions can be observed through the plots, but they do not alter the overall behavior. The inverse situation is true for data computed with λ_2, according to our discussion of Figure 6. Such a behavior is quite consistent with the benchmark system, as can be assessed by comparing Figure 8 with Figure 4.

On the other hand, relative error increases for all cases, with the noteworthy exception of $\bar{\lambda}_4$ that lies close to zero for all values of the ratio λ_1/λ_2 (Figure S5 can be used to understand this behavior), also the benchmark displays such a feature: the values calculated with $\bar{\lambda}_3$ and $\bar{\lambda}_4$ remain close to each other for smaller values of the ratio (in particular, it is shown for the interval $\lambda_1/\lambda_2 < 3$, see Figure 4). It can be observed that in most cases, the ratio between the λ's shows that one is twice the other at most; this situation prevails despite the dissimilarity of the considered molecules.

For the sake of completeness, we provide plots analogous to Figure 8 but with different references in the Supporting Information. Figures S6–S8 display the relative error data calculated when $\bar{\lambda}_1$, $\bar{\lambda}_2$, or $\bar{\lambda}_4$ are the references, respectively. Figures S9 and S10 display the data of λ_1 and λ_2 as references, respectively. The same trends discussed for Figure 8 can be recovered from these plots.

To end this section, we mention that in our exploration of the methylated D–A pairs, we found 43 systems (36% of the considered cases) with potential application to practical OPV devices because they presented activation barriers smaller or around 2 eV. We present these pairs and their activation energies in Table 4. Additionally, we display the energy differences predicted by the use of the geometric average, $\bar{\lambda}_3$, instead of the arithmetic one $\bar{\lambda}_1$, and we observe that in 16 cases, such a difference is larger than 10 meV.

We analyze the impact of using the geometric average on the ET reaction rate in these cases. For such a purpose, we

Table 4. D–A Pairs with Practical Relevance[a]

acceptor	donor	$\Delta G^{\dagger}(\bar{\lambda}_3)$	$\Delta\Delta G^{\dagger}$	$k(\bar{\lambda}_1)/k(\bar{\lambda}_3)$
A1	D6	0.662	0.018	2.02
	D4	1.918	0.007	1.31
	D7	0.807	0.005	1.21
	D8	2.025	0.012	1.60
	D10	1.379	0.021	2.27
A4	D6	1.212	0.008	1.37
	D7	1.403	0.006	1.26
	D10	2.045	0.028	2.97
A6	D1	0.207	−0.001	0.96
	D2	0.242	−0.001	0.96
	D3	0.291	0.000	1.00
	D5	1.560	0.003	1.12
	D8	1.878	0.000	1.00
	D9	1.810	0.005	1.21
	D10	2.088	0.061	10.75
A7	D6	1.508	0.000	1.00
	D7	1.737	0.000	1.00
A8	D2	2.034	0.015	1.79
	D4	1.362	0.002	1.08
	D5	1.814	0.001	1.04
	D6	0.366	0.001	1.04
	D7	0.473	0.000	1.00
	D8	1.470	0.001	1.04
	D9	2.143	0.010	1.48
	D10	0.980	0.030	3.22
A9	D6	0.945	0.014	1.72
	D7	1.132	0.011	1.53
	D10	1.770	0.027	2.86
A10	D4	1.878	0.000	1.00
	D6	0.675	0.000	1.00
	D7	0.818	0.000	1.00
	D8	1.990	0.000	1.00
	D10	1.413	0.050	7.01
A11	D6	1.693	0.047	6.23
	D7	1.955	0.042	5.13
A12	D2	1.967	0.003	1.12
	D4	1.313	0.002	1.08
	D5	1.807	0.019	2.10
	D6	0.297	0.001	1.04
	D7	0.402	0.002	1.08
	D8	1.426	0.004	1.17
	D9	2.149	0.000	1.00
	D10	0.947	0.068	14.12

[a]Predicted activation energy, $\Delta G^{\dagger}(\bar{\lambda}_3)$, differences in activation energy from two different averages, $\Delta\Delta G^{\dagger} = \Delta G^{\dagger}(\bar{\lambda}_3) - \Delta G^{\dagger}(\bar{\lambda}_1)$, and ratio of predicted rate constants at room T. All energies in electronvolt.

DOI: 10.1021/acsomega.7b01425
ACS Omega 2018, 3, 2130–2140

compute the ratio between the rate constant computed with the geometric average, $k(\overline{\lambda}_3)$, and the rate constant computed with the arithmetic average, $k(\overline{\lambda}_1)$, and present the results in the last column of Table 4. It can be observed that many of the predicted energetic differences should lead to experimentally detectable predictions in reaction rates because in many cases, the factor is two or more, with respect to those rates calculated with $\overline{\lambda}_1$.

Future work focused on finding species with practical relevance should consider several refinements of these data, as well as the study of different substituents. A remarkable refinement would be the consideration of quantum effects on the reaction rates, such as in the Marcus−Hush−Jortner[97−99] formalism. Also, the consideration of solvent effects on the reorganization energies through the inclusion of implicit solvent models could be important. It is worth to mention that all these effects may lower the computed energies and lead to technologically relevant findings.

CONCLUSIONS

The four-point Nelsen scheme to compute activation free energies through the Marcus−Hush theory was appraised in two different contexts with the purpose of explicitly considering differences in the curvatures of the parabolas involved. This situation is very common in its chemical and biological applications.

The first assessment was performed in the context of the aluminum dimer, Al_2, a system that can be solved analytically under the Marcus−Hush theory assumptions. We applied the four-point Nelsen scheme involving different averages of the calculated parabolic curvatures and then compared the results with the analytical solution. The main result of this part is that the geometric average $(\overline{\lambda}_3)$ and the composed average $(\overline{\lambda}_4)$ drastically diminish the error for all the considered values of the ratio between the curvatures.

For a second assessment on more realistic systems, we studied 120 D−A pairs with technological interest in the OPV field. For these systems, we employed the four-point Nelsen scheme to compute the free energy barriers associated with the ET reactions considering different averages of the internal reorganization energies and found that the computations strongly depend on our choice. In particular, our interest was focused on the predicted differences between the values calculated with the geometric and the arithmetic averages. We found that predicted differences can be quite significant. In all cases, an increase in the energetic barrier (slower ET) is predicted when the geometric averages are employed.

On the other hand, the overall trends displayed by both the geometric and arithmetic averages on the 120 considered data are very similar despite the differences predicted when each individual pair is considered. Despite the hard assumptions of this work, we found an improvement on the values that can be experimentally tested.

To validate our choice of $\overline{\lambda}_3$ as the most suitable quantity for the four-point Nelsen scheme, we built relative error plots for the 120 D−A pairs, using different references. All the relative error plots are very similar to those of the benchmark, showing the strong dependence of the error on the ratio of the reorganization energies. It must be stressed that this striking similarity occurs under the hard assumption that the only relevant feature is the ratio between the internal reorganization energies, hence dismissing any other feature of the molecular systems. In all cases, the obtained plots can be rationalized with the aid of Al_2, where the plotted values were computed analytically.

Finally, in 36% of the considered cases, we predict activation energies that may have practical relevance. Data calculated with $\overline{\lambda}_1$ and $\overline{\lambda}_3$ present reaction rates that are different enough as to be discriminated experimentally.

METHODS

D−A OPV Systems. The Gaussian 09 suite[95] was employed to perform the DFT computations. The exchange and correlation including dispersion ωB97XD[100] functional was employed. A correlation consistent triple-ζ basis set cc-pVTZ[101] was employed. A vibrational analysis was performed to verify the local minimum for each molecular geometry. As a first approximation, we only considered the nuclear harmonic contributions to the partition function for computation of the free Gibbs energy, and a future detailed treatment would evaluate the influence of anharmonicity on the results.

To get the relevant parameters of the left parabola, we optimized the neutral molecule to obtain $G_1(x_1)$, following Figure 1, and then performed a single-point calculation with this coordinates but changing the charge to get the anionic species to compute $G_2(x_1)$. For the right parabola, by an analogous procedure we obtain $G_2(x_2)$ and $G_1(x_2)$. We obtained the reorganization energies through eq 3 and then used them and their averages, in addition to the reaction driving force, ΔG^0, in eq 2 to get the corresponding activation energy barriers. In other words, what is needed to apply the presently proposed technique is to calculate the four-point Nelsen quantities and average them in the manner proposed by eq 10 or 11.

ASSOCIATED CONTENT

Supporting Information

The Supporting Information is available free of charge on the ACS Publications website at DOI: 10.1021/acsomega.7b01425.

Details and analysis of the aluminum dimer equations, energetic properties for the donor and acceptor molecules studied in this research, sample Gaussian input files, calculation of the activation energy of a selected D−A pair as an explicit example, and plots of relative error of the 120 D−A pairs with different references (PDF)

AUTHOR INFORMATION

Corresponding Authors

*E-mail: omar.lopez.e@gmail.com (O.L.-E.).
*E-mail: carlos.amador@unam.mx (C.A.-B.).

ORCID

Omar López-Estrada: 0000-0002-9395-334X
Humberto G. Laguna: 0000-0002-5565-1551

Notes

The authors declare no competing financial interest.

ACKNOWLEDGMENTS

The authors thank DGTIC-UNAM for computational resources provided under the projects SC16-1-IG-37 and LANCAD-UNAM-DGTIC-022. O.L.-E. would like to thank CONACyT-SENER-Fondo de Sustentabilidad Energética for the postdoctoral fellowship under project 245754. H.G.L. thanks the program "CONACyT-SENER-Sustentabilidad En-

DOI: 10.1021/acsomega.7b01425
ACS Omega 2018, 3, 2130−2140

ergética 2015−2016" for a posdoctoral fellowship. C.B.-F. thanks CONACyT for a graduate fellowship. This research was funded by CONACyT-SENER-Fondo de Sustentabilidad Energética under project 245754.

REFERENCES

(1) Qin, Y.; Cheng, C.; Geng, H.; Wang, C.; Hu, W.; Xu, W.; Shuai, Z.; Zhu, D. Efficient Ambipolar Transport Properties in Alternate Stacking Donor-Acceptor Complexes: From Experiment to Theory. *Phys. Chem. Chem. Phys.* **2016**, *18*, 14094−14103.
(2) Zhu, L.; Geng, H.; Yi, Y.; Wei, Z. Charge Transport in Organic Donor-Acceptor Mixed-Stack Crystals: the Role of Nonlocal Electron-Phonon Couplings. *Phys. Chem. Chem. Phys.* **2017**, *19*, 4418−4425.
(3) Zhang, J.; Xu, W.; Sheng, P.; Zhao, G.; Zhu, D. Organic Donor-Acceptor Complexes as Novel Organic Semiconductors. *Acc. Chem. Res.* **2017**, *50*, 1654−1662.
(4) Dereka, B.; Koch, M.; Vauthey, E. Looking at Photoinduced Charge Transfer Processes in the IR: Answers to Several Long-Standing Questions. *Acc. Chem. Res.* **2017**, *50*, 426−434.
(5) Marcus, R. A. On the Theory of Oxidation-Reduction Reactions Involving Electron Transfer. III. Applications to Data on the Rates of Organic Redox Reactions. *J. Chem. Phys.* **1957**, *26*, 872−877.
(6) Marcus, R. A. On the Theory of Oxidation-Reduction Reactions Involving Electron Transfer. II. Applications to Data on the Rates of Isotopic Exchange Reactions. *J. Chem. Phys.* **1957**, *26*, 867−871.
(7) Marcus, R. A. On the Theory of Oxidation−Reduction Reactions Involving Electron Transfer. V. Comparison and Properties of Electrochemical and Chemical Rate Constants. *J. Phys. Chem.* **1963**, *67*, 853−857.
(8) Marcus, R. A. On the Theory of Electron-Transfer Reactions. VI. Unified Treatment for Homogeneous and Electrode Reactions. *J. Chem. Phys.* **1965**, *43*, 679.
(9) Henstridge, M. C.; Laborda, E.; Compton, R. G. Asymmetric Marcus-Hush Model of Electron Transfer Kinetics: Application to the Voltammetry of Surface-Bound Redox Systems. *J. Electroanal. Chem.* **2012**, *674*, 90−96.
(10) Henstridge, M. C.; Laborda, E.; Rees, N. V.; Compton, R. G. Marcus-Hush-Chidsey Theory of Electron Transfer Applied to Voltammetry: A Review. *Electrochim. Acta* **2012**, *84*, 12−20.
(11) Laborda, E.; Henstridge, M. C.; Compton, R. G. Asymmetric Marcus Theory: Application to Electrode Kinetics. *J. Electroanal. Chem.* **2012**, *667*, 48−53.
(12) Laborda, E.; Henstridge, M. C.; Batchelor-McAuley, C.; Compton, R. G. Asymmetric Marcus−Hush Theory for Voltammetry. *Chem. Soc. Rev.* **2013**, *42*, 4894−4905.
(13) Paddon-Row, M. N. Orbital Interactions and Long-Range Electron Transfer. *Adv. Phys. Org. Chem.* **2003**, *38*, 1−85.
(14) Kubař, T.; Elstner, M. What Governs the Charge Transfer in DNA? The Role of DNA Conformation and Environment. *J. Phys. Chem. B* **2008**, *112*, 8788−8798.
(15) Woiczikowski, P. B.; Kubař, T.; Gutiérrez, R.; Caetano, R. A.; Cuniberti, G.; Elstner, M. Combined Density Functional Theory and Landauer Approach for Hole Transfer in DNA Along Classical Molecular Dynamics Trajectories. *J. Chem. Phys.* **2009**, *130*, 215104.
(16) Woiczikowski, P. B.; Steinbrecher, T.; Kubař, T.; Elstner, M. Nonadiabatic QM/MM Simulations of Fast Charge Transfer in Escherichia Coli DNA Photolyase. *J. Phys. Chem. B* **2011**, *115*, 9846−9863.
(17) Gray, H. B.; Winkler, J. R. Electron Transfer in Proteins. *Annu. Rev. Biochem.* **1996**, *65*, 537−561.
(18) Shin, Y.-g. K.; Newton, M. D.; Isied, S. S. Distance Dependence of Electron Transfer Across Peptides with Different Secondary Structures: The Role of Peptide Energetics and Electronic Coupling. *J. Am. Chem. Soc.* **2003**, *125*, 3722−3732.
(19) Wallrapp, F. H.; Voityuk, A. A.; Guallar, V. Temperature Effects on Donor-Acceptor Couplings in Peptides. A Combined Quantum Mechanics and Molecular Dynamics Study. *J. Chem. Theory Comput.* **2010**, *6*, 3241−3248.
(20) Heck, A.; Woiczikowski, P. B.; Kubař, T.; Giese, B.; Elstner, M.; Steinbrecher, T. B. Charge Transfer in Model Peptides: Obtaining Marcus Parameters from Molecular Simulation. *J. Phys. Chem. B* **2012**, *116*, 2284−2293.
(21) Hervás, M.; Navarro, J. A.; De La Rosa, M. A. Electron Transfer Between Membrane Complexes and Soluble Proteins in Photosynthesis. *Acc. Chem. Res.* **2003**, *36*, 798−805.
(22) Bixon, M.; Jortner, J. *Electron Transfer—from Isolated Molecules to Biomolecules*; John Wiley & Sons, 1999; pp 35−202.
(23) Skourtis, S. S.; Waldeck, D. H.; Beratan, D. N. Fluctuations in Biological and Bioinspired Electron-Transfer Reactions. *Annu. Rev. Phys. Chem.* **2010**, *61*, 461−485.
(24) He, S.; Barco, R. A.; Emerson, D.; Roden, E. E. Comparative Genomic Analysis of Neutrophilic Iron(II) Oxidizer Genomes for Candidate Genes in Extracellular Electron Transfer. *Front. Microbiol.* **2017**, *8*, 1584.
(25) Olson, M.; Mao, Y.; Windus, T.; Kemp, M.; Ratner, M.; Léon, N.; Mujica, V. A Conformational Study of the Influence of Vibrations on Conduction in Molecular Wires. *J. Phys. Chem. B* **1998**, *102*, 941−947.
(26) Grozema, F. C.; Berlin, Y. A.; Siebbeles, L. D. A. Mechanism of Charge Migration through DNA: Molecular Wire Behavior, Single-step Tunneling or Hopping? *J. Am. Chem. Soc.* **2000**, *122*, 10903−10909.
(27) Ishikawa, T.; Hayes, S. A.; Keskin, S.; Corthey, G.; Hada, M.; Pichugin, K.; Marx, A.; Hirscht, J.; Shionuma, K.; Onda, K.; et al. Direct Observation of Collective Modes Coupled to Molecular Orbital-driven Charge Transfer. *Science* **2015**, *350*, 1501−1506.
(28) Delor, M.; Scattergood, P. A.; Sazanovich, I. V.; Parker, A. W.; Greetham, G. M.; Meijer, A. J. H. M.; Towrie, M.; Weinstein, J. A. Toward Control of Electron Transfer in Donor-acceptor Molecules by Bond-specific Infrared Excitation. *Science* **2014**, *346*, 1492−1495.
(29) Delor, M.; Keane, T.; Scattergood, P. A.; Sazanovich, I. V.; Greetham, G. M.; Towrie, M.; Meijer, A. J. H. M.; Weinstein, J. A. On the Mechanism of Vibrational Control of Light-induced Charge Transfer in Donor-bridge-acceptor Assemblies. *Nat. Chem.* **2015**, *7*, 689−695.
(30) Bakulin, A. A.; Lovrincic, R.; Yu, X.; Selig, O.; Bakker, H. J.; Rezus, Y. L. A.; Nayak, P. K.; Fonari, A.; Coropceanu, V.; Brédas, J.-L.; et al. Mode-selective Vibrational Modulation of Charge Transport in Organic Electronic Devices. *Nat. Commun.* **2015**, *6*, 7880.
(31) Nelson, J.; Kwiatkowski, J. J.; Kirkpatrick, J.; Frost, J. M. Modeling Charge Transport in Organic Photovoltaic Materials. *Acc. Chem. Res.* **2009**, *42*, 1768−1778.
(32) Liu, T.; Cheung, D. L.; Troisi, A. Structural Variability and Dynamics of the P3HT/PCBM Interface and its Effects on the Electronic Structure and the Charge-transfer Rates in Solar Cells. *Phys. Chem. Chem. Phys.* **2011**, *13*, 21461−21470.
(33) Ren, G.; Ahmed, E.; Jenekhe, S. A. Non-fullerene Acceptor-based Bulk Heterojunction Polymer Solar Cells: Engineering the Nanomorphology via Processing Additives. *Adv. Energy Mater.* **2011**, *1*, 946−953.
(34) Si, Y.; Liang, W.; Zhao, Y. Theoretical Prediction of Triplet−Triplet Energy Transfer Rates in a Benzophenone−Fluorene−Naphthalene System. *J. Phys. Chem. C* **2012**, *116*, 12499−12507.
(35) Zhang, W.; Zhong, X.; Zhao, Y. Electron Mobilities of n-Type Organic Semiconductors from Time-Dependent Wavepacket Diffusion Method : Pentacenequinone Derivatives. *J. Phys. Chem. A* **2012**, *116*, 11075−11082.
(36) Anne, F. B.; Galland, N.; Jacquemin, D. Computing Redox Potentials for Dyes Used in p-type dye-sensitized Solar Cells. *Int. J. Quantum Chem.* **2012**, *112*, 3763−3768.
(37) Leng, C.; Qin, H.; Si, Y.; Zhao, Y. Theoretical Prediction of the Rate Constants for Exciton Dissociation and Charge Recombination to a Triplet State in PCPDTBT with Different Fullerene Derivatives. *J. Phys. Chem. C* **2014**, *118*, 1843−1855.
(38) Lee, M. H.; Dunietz, B. D.; Geva, E. Calculation from First Principles of Intramolecular Golden-Rule Rate Constants for Photo-

DOI: 10.1021/acsomega.7b01425
ACS Omega 2018, 3, 2130−2140

Induced Electron Transfer in Molecular Donor−Acceptor Systems. *J. Phys. Chem. C* **2013**, *117*, 23391−23401.
(39) Zhang, W.; Chen, X.; Liang, W.; Zhao, Y. Electron Transfer Pathways in the Z-schematic Donor-donor-acceptor Organic Solar Cells. *Commun. Comput. Chem.* **2013**, *1*, 132−144.
(40) Scharber, M. C.; Sariciftci, N. S. Efficiency of Bulk-heterojunction Organic Solar Cells. *Prog. Polym. Sci.* **2013**, *38*, 1929−1940.
(41) Shuai, Z.; Geng, H.; Xu, W.; Liao, Y.; André, J.-M. From Charge Transport Parameters to Charge Mobility in Organic Semiconductors through Multiscale Simulation. *Chem. Soc. Rev.* **2014**, *43*, 2662.
(42) Aquino, A. A. J.; Borges, I.; Nieman, R.; Köhn, A.; Lischka, H. Intermolecular Interactions and Charge Transfer Transitions in Aromatic Hydrocarbon−Tetracyanoethylene Complexes. *Phys. Chem. Chem. Phys.* **2014**, *16*, 20586−20597.
(43) Zhong, X.; Zhao, Y.; Cao, J. Coherent Quantum Transport in Disordered Systems: II. Temperature Dependence of Carrier Diffusion Coefficients from the Time-Dependent Wavepacket Diffusion Method. *New J. Phys.* **2014**, *16*, 045009.
(44) Van den Brande, N.; Van Lier, G.; Da Pieve, F.; Van Assche, G.; Van Mele, B.; De Proft, F.; Geerlings, P. A Time Dependent DFT Study of the Efficiency of Polymers for Organic Photovoltaics at the Interface with PCBM. *RSC Adv.* **2014**, *4*, 52658−52667.
(45) Huang, J.-D.; Li, W.-L.; Wen, S.-H.; Dong, B. Electronic Structure and Microscopic Charge-Transport Properties of a New-type Diketopyrrolopyrrole-based Material. *J. Comput. Chem.* **2015**, *36*, 695−706.
(46) Chen, L.; Shenai, P.; Zheng, F.; Somoza, A.; Zhao, Y. Optimal Energy Transfer in Light-Harvesting Systems. *Molecules* **2015**, *20*, 15224−15272.
(47) Wright, B. F.; Sunahara, K.; Furube, A.; Nattestad, A.; Clarke, T. M.; Bazan, G. C.; Azoulay, J. D.; Mozer, A. J. Driving Force Dependence of Electron Transfer Kinetics and Yield in Low-Band-Gap Polymer Donor−Acceptor Organic Photovoltaic Blends. *J. Phys. Chem. C* **2015**, *119*, 12829−12837.
(48) Pelzer, K. M.; Darling, S. B. Charge Generation in Organic Photovoltaics: A Review of Theory and Computation. *Mol. Syst. Des. Eng.* **2016**, *1*, 10−24.
(49) Zhang, C.-Z.; Shen, D.; Yuan, Y.; Song, M.-X.; Li, S.-J.; Cao, H. Syntheses of Planar 1,5,2,4,6,8-dithiotetrazocine Derivatives and Thermodynamic Study on Intermolecular Charge Transfer for Developing Efficient Organic Solar Cell. *Mater. Chem. Phys.* **2016**, *177*, 463−471.
(50) Brückner, C.; Würthner, F.; Meerholz, K.; Engels, B. Atomistic Approach to Simulate Processes Relevant for the Efficiencies of Organic Solar Cells as a Function of Molecular Properties. II. Kynetics Aspects. *J. Phys. Chem. C* **2017**, *121*, 26−51.
(51) Goldey, M. B.; Reid, D.; de Pablo, J.; Galli, G. Planarity and Multiple Components Promote Organic Photovoltaic Efficiency by improving Electronic Transport. *Phys. Chem. Chem. Phys.* **2016**, *18*, 31388.
(52) Gao, L.; Zhang, Z.-G.; Bin, H.; Xue, L.; Yang, Y.; Wang, C.; Liu, F.; Russell, T. P.; Li, Y. High-Efficiency Nonfullerene Polymer Solar Cells with Medium Bandgap Polymer Donor and Narrow Bandgap Organic Semiconductor Acceptor. *Adv. Mater.* **2016**, *28*, 8288−8295.
(53) Xu, B.; Li, Y.; Song, P.; Ma, F.; Sun, M. Photoactive Layer Based on T-shaped Benzimidazole Dyes Used for Solar Cell: From Photoelectric Properties to Molecular Design. *Sci. Rep.* **2017**, *7*, 45688.
(54) Zheng, Z.; Tummala, N. R.; Fu, Y.-T.; Coropceanu, V.; Brédas, J.-L. Charge-Transfer States in Organic Solar Cells: Understanding the Impact of Polarization, Delocalization, and Disorder. *ACS Appl. Mater. Interfaces* **2017**, *9*, 18095−18102.
(55) Singh, R.; Lee, J.; Kim, M.; Keivanidis, P. E.; Cho, K. Control of the Molecular Geometry and Nanoscale Morphology in Perylene Diimide Based Bulk Heterojunctions Enables an Efficient Non-fullerene Organic Solar Cell. *J. Mater. Chem. A* **2017**, *5*, 210−220.
(56) Marcus, R. A. Chemical and Electrochemical Electron-Transfer Theory. *Annu. Rev. Phys. Chem.* **1964**, *15*, 155−196.
(57) Marcus, R. A.; Sutin, N. Electron Transfers in Chemistry and Biology. *Biochim. Biophys. Acta* **1985**, *811*, 265−322.
(58) Hush, N. S. Adiabatic Rate Processes at Electrodes. I. Energy-Charge Relationships. *J. Chem. Phys.* **1958**, *28*, 962−972.
(59) Hush, N. S. Electron transfer in retrospect and prospect 1: Adiabatic electrode processes. *J. Electroanal. Chem.* **1999**, *470*, 170−195.
(60) Kuss-Petermann, M.; Wenger, O. S. Increasing Electron-Transfer Rates with Increasing Donor-Acceptor Distance. *Angew. Chem., Int. Ed.* **2016**, *55*, 815−819.
(61) Wasielewski, M. R.; Niemczyk, M. P.; Svec, W. A.; Pewitt, E. B. Dependence of Rate Constants for Photoinduced Charge Separation and Dark Charge Recombination on the Free Energy of Reaction in Restricted-distance Porphyrin-quinone Molecules. *J. Am. Chem. Soc.* **1985**, *107*, 1080−1082.
(62) Closs, G. L.; Miller, J. R. Intramolecular Long-Distance Electron Transfer in Organic Molecules. *Science* **1988**, *240*, 440−447.
(63) Zhou, H.-X.; Szabo, A. Microscopic Formulation of Marcus' Theory of Electron Transfer. *J. Chem. Phys.* **1995**, *103*, 3481−3494.
(64) Zwickl, J.; Shenvi, N.; Schmidt, J. R.; Tully, J. C. Transition State Barriers in Multidimensional Marcus Theory. *J. Phys. Chem. A* **2008**, *112*, 10570−10579.
(65) Matyushov, D. V.; Voth, G. A. Modeling the Free Energy Surfaces of Electron Transfer in Condensed Phases. *J. Chem. Phys.* **2000**, *113*, 5413−5424.
(66) Small, D. W.; Matyushov, D. V.; Voth, G. A. The Theory of Electron Transfer Reactions: What May Be Missing? *J. Am. Chem. Soc.* **2003**, *125*, 7470−7478.
(67) Vuilleumier, R.; Tay, K. A.; Jeanmairet, G.; Borgis, D.; Boutin, A. Extension of Marcus Picture for Electron Transfer Reactions with Large Solvation Changes. *J. Am. Chem. Soc.* **2012**, *134*, 2067−2074.
(68) Hupp, J. T.; Weaver, M. J. The Driving-Force Dependence of Electrochemical Rate Parameters: Origins of Anodic-Cathodic Asymmetries for Metal-Aquo Redox Couples. *J. Phys. Chem.* **1984**, *88*, 6128−6135.
(69) Hupp, J. T.; Weaver, M. J. Prediction of Electron-Transfer Reactivities from Contemporary Theory: Unified Comparisons for Electrochemical and Homogeneous Reactions. *J. Phys. Chem.* **1985**, *89*, 2795−2804.
(70) Warshel, A. Dynamics of Reactions in Polar Solvents. Semiclassical Trajectory Studies of Electron-Transfer and Proton-Transfer Reactions. *J. Phys. Chem.* **1982**, *86*, 2218−2224.
(71) Troisi, A.; Ratner, M. A.; Zimmt, M. B. Dynamic Nature of the Intramolecular Electronic Coupling Mediated by a Solvent Molecule: A Computational Study. *J. Am. Chem. Soc.* **2004**, *126*, 2215−2224.
(72) Wu, Q.; Van Voorhis, T. Constrained Density Functional Theory and its Application in Long-range Electron Transfer. *J. Chem. Theory Comput.* **2006**, *2*, 765−774.
(73) Wu, Q.; Van Voorhis, T. Extracting Electron Transfer Coupling Elements from Constrained Density Functional Theory. *J. Chem. Phys.* **2006**, *125*, 164105.
(74) Oberhofer, H.; Blumberger, J. Electronic Coupling Matrix Elements from Charge Constrained Density Functional Theory Calculations Using a Plane Wave Basis Set. *J. Chem. Phys.* **2010**, *133*, 244105.
(75) Migliore, A.; Nitzan, A. Nonlinear Charge Transport in Redox Molecular Junctions: A Marcus Perspective. *ACS Nano* **2011**, *5*, 6669−6685.
(76) Zhao, Y.; Liang, W. Charge Transfer in Organic Molecules for Solar Cells: Theoretical Perspective. *Chem. Soc. Rev.* **2012**, *41*, 1075−1087.
(77) Nelsen, S. F.; Blackstock, S. C.; Kim, Y. Estimation of Inner Shell Marcus Terms for Amino Nitrogen Compounds by Molecular Orbital Calculations. *J. Am. Chem. Soc.* **1987**, *109*, 677−682.
(78) Rauhut, G.; Clark, T. Electron-Transfer Reactions: AM1 and ab initio Studies on Self-Exchange in p-diaminobenzene Systems. *J. Am. Chem. Soc.* **1993**, *115*, 9127−9135.
(79) Nelsen, S. F.; Adamus, J.; Wolff, J. J. Comparison of Intramolecular Electron Transfer Rate Constant with Hush Theory

DOI: 10.1021/acsomega.7b01425
ACS Omega 2018, 3, 2130−2140

for an Organic Intervalence Compound. *J. Am. Chem. Soc.* **1994**, *116*, 1589−1590.
(80) Blomgren, F.; Larsson, S.; Nelsen, S. F. Electron Transfer in bis(hydrazines), a Critical Test for Application of the Marcus Model. *J. Comput. Chem.* **2001**, *22*, 655−664.
(81) Siriwong, K.; Voityuk, A. A.; Newton, M. D.; Rösch, N. Estimate of the Reorganization Energy for Charge Transfer in DNA. *J. Phys. Chem. B* **2003**, *107*, 2595−2601.
(82) Nelsen, S. F.; Weaver, M. N.; Konradsson, A. E.; Telo, J. P.; Clark, T. Electron Transfer within 2,7-dinitronaphthalene Radical Anion. *J. Am. Chem. Soc.* **2004**, *126*, 15431−15438.
(83) Rosso, K. M.; Dupuis, M. Reorganization Energy Associated with Small Polaron Mobility in Iron Oxide. *J. Chem. Phys.* **2004**, *120*, 7050−7054.
(84) Nelsen, S. F.; Weaver, M. N.; Luo, Y.; Pladziewicz, J. R.; Ausman, L. K.; Jentzsch, T. L.; O'Konek, J. J. Estimation of Electronic Coupling for Intermolecular Electron Transfer from Cross-Reaction Data. *J. Phys. Chem. A* **2006**, *110*, 11665−11676.
(85) Rosso, K. M.; Dupuis, M. Electron Transfer in Environmental Systems: A Frontier for Theoretical Chemistry. *Theor. Chem. Acc.* **2006**, *116*, 124−136.
(86) Rosokha, S. V.; Kochi, J. K. Continuum of outer- and inner-sphere Mechanisms for Organic Electron Transfer. Steric Modulation of the Precursor Complex in Paramagnetic (ion-radical) self-exchanges. *J. Am. Chem. Soc.* **2007**, *129*, 3683−3697.
(87) Zhang, W.; Zhu, W.; Liang, W.; Zhao, Y.; Nelsen, S. F. Ab initio calculations on the intramolecular electron transfer rates of a bis(hydrazine) radical cation. *J. Phys. Chem. B* **2008**, *112*, 11079−11086.
(88) Markle, T. F.; Mayer, J. M. Concerted Proton-Electron Transfer in Pyridylphenols: The Importance of the Hydrogen Bond. *Angew. Chem., Int. Ed.* **2008**, *47*, 738−740.
(89) Evans, D. H. One-electron and Two-electron Transfers in Electrochemistry and Homogeneous Solution Reactions. *Chem. Rev.* **2008**, *108*, 2113−2144.
(90) Chang, Y.-C.; Chao, I. An Important Key to Design Molecules with Small Internal Reorganization Energy: Strong Nonbonding Character in Frontier Orbitals. *J. Phys. Chem. Lett.* **2010**, *1*, 116−121.
(91) Fu, Z.; Lemire, G. W.; Bishea, G. A.; Morse, M. D. Spectroscopy and Electronic Structure of Jet-cooled Al_2. *J. Chem. Phys.* **1990**, *93*, 8420−8441.
(92) López-Estrada, O.; Orgaz, E. Theoretical Study of the Spin Competition in Small-Sized Al Clusters. *J. Phys. Chem. A* **2015**, *119*, 11941−11948.
(93) Perdew, J. P.; Burke, K.; Ernzerhof, M. Generalized Gradient Approximation Made Simple. *Phys. Rev. Lett.* **1996**, *77*, 3865−3868.
(94) Schäfer, A.; Huber, C.; Ahlrichs, R. Fully Optimized Contracted Gaussian Basis Sets of Triple Zeta Valence Quality for Atoms Li to Kr. *J. Chem. Phys.* **1994**, *100*, 5829−5835.
(95) Frisch, M. J.; Trucks, G. W.; Schlegel, H. B.; Scuseria, G. E.; Robb, M. A.; Cheeseman, J. R.; Scalmani, G.; Barone, V.; Mennucci, B.; Petersson, G. A.; et al. *Gaussian 09*, Revision E.01; Gaussian Inc.: Wallingford, CT, 2009.
(96) Das, A.; Ghosh, S. Supramolecular Assemblies by Charge-Transfer Interactions Between Donor and Acceptor Chromophores. *Angew. Chem., Int. Ed.* **2014**, *53*, 2038−2054.
(97) Bixon, M.; Jortner, J. Intramolecular Radiationless Transitions. *J. Chem. Phys.* **1968**, *48*, 715.
(98) Ulstrup, J.; Jortner, J. The Effect of Intramolecular Quantum Modes on Free Energy Relationships for Electron Transfer Reactions. *J. Chem. Phys.* **1975**, *63*, 4358−4368.
(99) Bixon, M.; Jortner, J. Quantum Effects on Electro-tranfer Processes. *Faraday Discuss. Chem. Soc.* **1982**, *74*, 17−29.
(100) Chai, J.-D.; Head-Gordon, M. Long-range Corrected Hybrid Density Functionals with Damped Atom-Atom Dispersion Corrections. *Phys. Chem. Chem. Phys.* **2008**, *10*, 6615.
(101) Kendall, R. A., Jr.; Dunning, T. H.; Harrison, R. J. Electron Affinities of the First-row Atoms Revisited. Systematic Basis Sets and Wave Functions. *J. Chem. Phys.* **1992**, *96*, 6796−6806.

DOI: 10.1021/acsomega.7b01425
ACS Omega 2018, 3, 2130−2140